Journal of
Ceramic Science
and Technology

J. Ceram. Sci. Tech., 07 [03] 257-262 (2016)
DOI: 10.4416/JCST2016-00001
available online at: http://www.ceramic-science.com

Crystal Structure, Raman Spectra and Dielectric Properties of $Ca_{0.66}Ti_{0.66}La_{0.34}Al_{0.34}O_3$ Microwave Ceramics with Nd^{3+}Additions

Y. Xu, R. Fu*, Y. Yang, J. Cai, X. Gu, J. Fang

College of Materials Science and Technology, Nanjing University of Aeronautics and Astronautics, 210016, Nanjing, Jiangsu

received January 3, 2016; received in revised form February 22, 2016; accepted April 13, 2016

Abstract

$Ca_{0.66}Ti_{0.66}La_{0.34}Al_{0.34}O_3$ (CTLA) ceramics doped with Nd_2O_3 were prepared by means of the conventional solid-state reaction method. The Nd_2O_3 dopant was added in the range of 0.5 – 3.5 wt%. The dielectric properties, crystal structure and Raman spectra of the CTLA ceramics doped with Nd_2O_3 were investigated with the Hakki and Coleman's dielectric resonant, XRD and Raman spectroscopy method, respectively. It was found that Nd_2O_3 promotes the densification and enlarges the crystal cell volume of CTLA ceramics. Two chemical reaction defects emerge in CTLA ceramics with the substitution of Nd^{3+}. Nd^{3+} is substituted for La/Ca atoms at the A-sites of the CTLA ceramics' structure with increasing Nd_2O_3 doping, and the polarization of the TiO_6 octahedra reaches the maximum volume when the amount of Nd_2O_3doping is 2.0 wt%. Excellent microwave dielectric properties of $Q\times f$= 37454 GHz (@4 GHz), ε_r = 45 and τ_f = 0.13 ppm/°C were obtained for CTLA ceramics with the addition of 2.0 wt% Nd_2O_3.

Keywords: $Ca_{0.66}Ti_{0.66}La_{0.34}Al_{0.34}O_3$, microwave dielectric properties, structure, additives

I. Introduction

Microwave dielectric materials are widely used in resonators, filters and integrated passive modules for developing wireless communications applications [1–3]. Dielectric constant (ε_r), quality factor ($Q\times f$), and temperature coefficient of the resonant frequency (τ_f) are three key parameters of microwave dielectric materials [4–6]. Most microwave dielectric ceramics with low and medium permittivity are perovskite-type ceramics, which usually have a high quality factor and good temperature-stable properties [7]. Moreover, the versatility of the perovskite structure provides the possibility for making solid solutions to meet specific requirements. The dielectric properties of solid solutions could be compatible with their crystal structures, tolerance factor and processing conditions [8].

Orthorhombic-distorted perovskite-type $CaTiO_3$ ceramics have high relative permittivity (ε_r = 170), a modest quality factor ($Q\times f$ = 3500 GHz), but a very high positive temperature coefficient of resonant frequency (τ_f = +800 ppm/°C) [9]. They are composited with $LaAlO_3$, which has low relative permittivity (ε_r = 23.4), a high quality factor ($Q\times f$ = 68 000 GHz) and a negative temperature coefficient of resonant frequency (τ_f = -44 ppm/°C) [10]. The high positive τ_f of $CaTiO_3$ can be suppressed to lower values and even near to zero when composited with $LaAlO_3$ [11,12], while the $CaTiO_3$ ceramics retain their high quality factor. Suvorov *et al.* reported that 70 mol% $CaTiO_3$ composited with 30 mol% $LaAlO_3$ achieved excellent dielectric properties of ε_r = 44, $Q\times f$ = 30 000 GHz and τ_f =15 ppm/°C [13]. Soon after, some researchers found that the dielectric properties and densification could be improved by increasing the LA($LaAlO_3$) or Al_2O_3 content in CTLA ceramics [14,15]. Furthermore, the alkaline-earth elements or rare earth elements substituted for A site ions in the perovskite structure, such as Ca^{2+} in CTLA ceramics, could improve the dielectric properties of perovskite ceramics too [16].

In the present study, $Ca_{0.66}Ti_{0.66}La_{0.34}Al_{0.34}O_3$ ceramics were chosen as the target perovskite-structure ceramics, and Nd_2O_3 was chosen as a new additive to improve the dielectric properties of the CTLA ceramics. The influence of the Nd_2O_3 additive on the microwave dielectric properties and microstructure of CTLA ceramics was investigated with the Hakki and Coleman's dielectric resonant, SEM, XRD and Raman spectroscopy method. The development of microstructures and microwave dielectric properties of the CTLA ceramics were demonstrated.

II. Experiments

(1) Sample preparation

Samples were synthesized by means of the conventional solid-state reaction. Reagent-grade $CaCO_3$, Nd_2O_3, TiO_2, La_2O_3, and Al_2O_3 with purity of over 99.9 wt% (Sinopharm Chemical Reagent Co., Ltd, Shanghai, China) were used as starting materials. The powders were weighed according to the stoichiometry ($Ca_{0.66}Ti_{0.66}La_{0.34}Al_{0.34}O_3$) and ball-milled for 20 h in a nylon jar using deionized water and zirconia media, dried at 110 °C and forced through a 60-mesh sieve. The $Ca_{0.66}Ti_{0.66}La_{0.34}Al_{0.34}O_3$ ceramics were calcined

* Corresponding author: renlifu@nuaa.edu.cn

at 1200 °C for 4 h, then different amounts of Nd_2O_3 were added to the calcined $Ca_{0.66}Ti_{0.66}La_{0.34}Al_{0.34}O_3$ according to Table 1. The resulting powders were wet-milled for 10 h and dried. The dried and granulated powders were pressed into discs measuring 15 mm in diameter and 7 – 10 mm in thickness, and then sintered at 1450 °C for 4 h in air.

Table 1: The formula of the experiment.

Simple NO.	(a)	(b)	(c)	(d)	(e)	(f)	(g)	(h)
Matrix material	The calcined $Ca_{0.66}Ti_{0.66}La_{0.34}Al_{0.34}O_3$							
Amounts of Nd_2O_3(wt%)	0	0.5	1.0	1.5	2.0	2.5	3.0	3.5

(2) Dielectric properties

The dielectric properties were measured with the Hakki and Coleman's dielectric resonant method under TE_{011} and $TE_{01\delta}$ modes with an Advantest R3767C network analyzer. The τ_f was measured at 4.0 GHz in the temperature range of 25 – 85 °C. The densities of the sintered specimens were measured with the Archimedes' method.

(3) X-ray diffraction

XRD measurements of the samples were performed on a computerized Bruker D8 advanced X diffractometer using CuKα (λ = 0.1542 nm) radiation. The XRD diffraction patterns were taken in the 2θ range of 10 – 80° at a scan speed of 0.02°/s.

(4) Scanning electron microscopy (SEM)

Microstructural examination of the sintered ceramics was performed by means of scanning electron microscopy (SEM) (Hitachi SU8010 and PHILIPS XL30). The sintered surfaces of ceramics were ground (to 1200 grade SiC) and polished (to 1-μm diamond paste). The samples were then thermally etched at 1350 °C for 60 min and coated with Au prior to SEM analysis.

(5) Raman spectroscopy

The Raman spectra were captured at room temperature on polished samples with a Raman spectrometer (inVia Reflex Raman Microscope). The laser line at 523 nm of a helium-neon ion laser was used as an excitation source with an elective power of 17 mW.

III. Results and Discussion

(1) X-ray diffraction (XRD) analysis

Fig. 1 shows the XRD patterns of CTLA ceramics with different amounts of Nd_2O_3 doping (sintered at 1450 °C for 4 h). All of the samples doped with different amounts of Nd_2O_3 have the same diffraction patterns except the position of diffraction peaks. This means that doping with Nd_2O_3 had little influence on the CTLA crystal structure. However, the diffraction peak (200) of the CTLA ceramics shifts to a lower 2θ angle as the doping of Nd_2O_3 increases up to 2.0 wt%, and then gradually shifts to a higher 2θ angle.

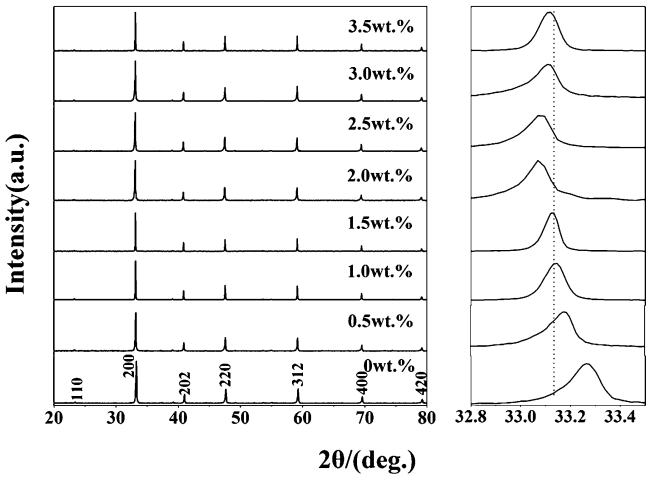

Fig. 1: XRD patterns of CTLA ceramics with different amounts ofNd_2O_3 sintered at 1450 °C for 4 h. (a) 0 wt%; (b) 0.5 wt%; (c) 1.0 wt%; (d) 1.5 wt%; (e) 2.0 wt%; (f) 2.5 wt%; (g) 3.0 wt%; (h) 3.5 wt%.

In the perovskite-type ceramics structure, there are three types of cation sites [17]. The La/Ca atoms occupy the A sites, the Ti/Al atoms occupy the B sites in the structure of CTLA ceramics, as shown in Fig. 2. The ionic radii of Nd^{3+} and Ca^{2+} are 0.98 Å and 0.99 Å [18], respectively, according to the principles of ionic radius tolerance in perovskite-type ceramics, Nd^{3+} ions would like to substitute for Ca^{2+} cations in the A-site of the CTLA ceramics. With increasing Nd^{3+} doping, the Nd^{3+} substitutes for La^{3+} cations at the A-site of the CTLA ceramics. The above substitution processes can be interpreted as the following defect chemistry reactions:

$$2TiO_2 + Nd_2O_3 \rightarrow 2Nd_{Ca}^{\cdot} + 2e' + 2Ti_{Ti}^{\times} + 6O_O^{\times} + \frac{1}{2}O_2 \quad (1)$$

$$Al_2O_3 + Nd_2O_3 \rightarrow 2Nd_{La}^{\times} + 2Al_{Al}^{\times} + 6O^{\times} \quad (2)$$

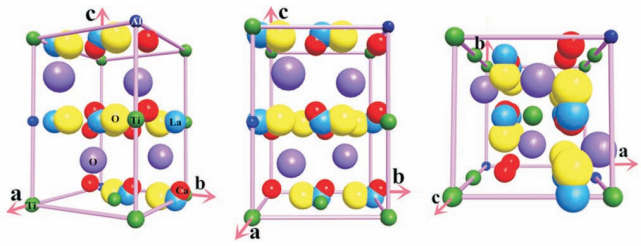

Fig. 2: The structure of CTLA ceramics viewed along three different directions.

In order to understand these substitution processes, the diagram of Nd^{3+} substituted for Ca^{2+} and La^{3+} in the CTLA ceramics is shown in Fig. 3. The Nd^{3+} ions substitute for Ca^{2+} at the A-site of the CTLA structure when the Nd doping amounts to less than 1 wt%. The Nd^{3+} could substitute for La^{3+} ions at A-site of the CTLA ceramic structure when doping of Nd^{3+} amounts to more than 2 wt%. The structure refinement of CTLA ceramics doped with different amounts of Nd_2O_3 is shown in Table 2.

Table 2: The structure refinement of CTLA ceramics doped with different amounts of Nd_2O_3.

Sample	Atom	x	y	z	Occupancy
0 wt%Nd_2O_3	Ca	1.01016	0.01535	1/4	0.66
	La	1.00336	0.02429	1/4	0.34
1 wt% Nd_2O_3	Ca	1.01016	0.01535	1/4	0.65
	La	1.00336	0.02429	1/4	0.34
	Nd	1.01016	0.01535	1/4	0.01
3 wt%Nd_2O_3	Ca	1.01016	0.01535	1/4	0.64
	La	1.00336	0.02429	1/4	0.33
	Nd1	1.01016	0.01535	1/4	0.02
	Nd2	1.00336	0.02429	1/4	0.01

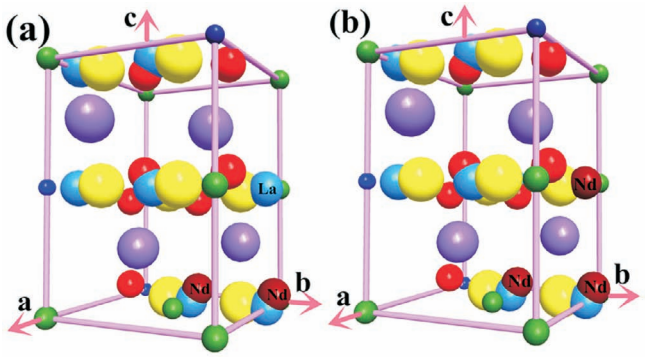

Fig. 3: The defect of chemical reaction of CTLA ceramics with different amounts of Nd_2O_3: (a)A small amount of Nd doping (b)A large amount of Nd doping.

(2) *Densification*

The relative density of CTLA ceramics with different amounts of Nd_2O_3 sintered at 1450 °C for 4 h is shown in Fig. 4. The relative density of undoped CTLA ceramics is only 94.4 %. The relative density of CTLA ceramics is clearly improved with Nd_2O_3 addition. Moreover, the relative density of ceramics increases until it reaches a maximum value before it then decreases with a further increase in Nd_2O_3. The highest relative density is 96.5 % at 2 wt% Nd_2O_3.

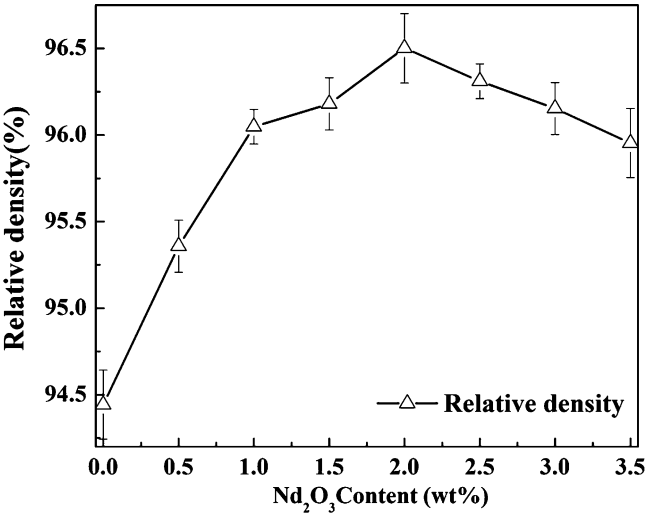

Fig. 4: The relative densities of CTLA ceramics with different amounts of Nd_2O_3 sintered at 1450 °C for 4 h.

(3) *Microwave dielectric properties*

The Q×f values and dielectric constant of the CTLA ceramics with different amounts of Nd_2O_3 sintered at 1450 °C for 4 h are shown in Fig. 5. The Q×*f* of undoped CTLA ceramics is only 36718.76 GHz. The Q×*f* of CTLA ceramics is clearly improved with Nd_2O_3. Moreover, the Q×*f* of the ceramics increases until it reaches a maximum value at 2.0 wt% Nd_2O_3, before it decreases with a further increase in the addition of Nd_2O_3. The highest Q×*f* is 37454.6 GHz at 2.0 wt% Nd_2O_3. The peak in Q×*f* coincides with maximum densification, demonstrating the importance of high density. These results are also in agreement with the study of Huang Jing *et al.*, the addition of Ln (rare earth element) is an effective method for the improvement of microwave dielectric properties [19].

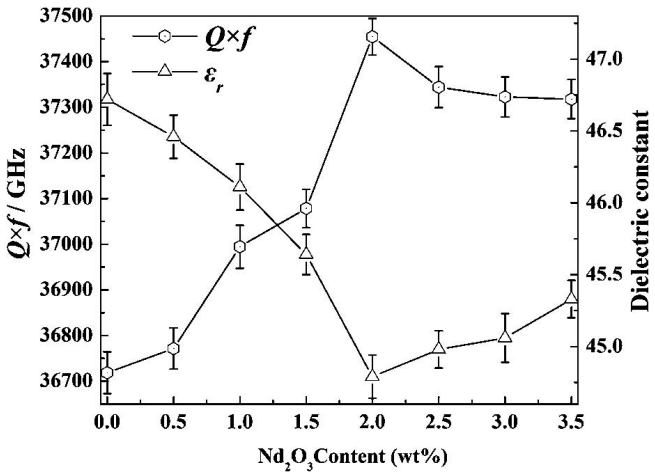

Fig. 5: The Q×f values and dielectric constant of CTLA ceramics with different amounts of Nd_2O_3sintered at 1450 °C for 4 h.

The dielectric constant of the CTLA ceramics with different amounts of Nd_2O_3 was similar to the change in the relative density and crystal cell volume. This change also proved that the crystal structure influences the microwave dielectric properties. The dielectric constant achieved the lowest value with the addition of 2.0 wt% Nd_2O_3.

The τ_f value of CTLA ceramics achieved zero with 2.0 wt% Nd_2O_3 additive, as the τ_f value of Nd_2O_3 is negative. However, with the addition of more than 2.0 wt%

Nd_2O_3, the τ_f value of CTLA ceramics does not decrease to the negative, otherwise τ_f value will increase to the positive again. The τ_f value can be adjusted by changing the cell polarization for the dielectric constant. The cell polarization can be calculated with the Clausius-Mossotti equation:

$$\frac{\varepsilon - 1}{\varepsilon + 2} = b\left(\frac{\chi}{V}\right) \quad (3)$$

where V is the crystal cell volume in $Å^3$, b is defined as $4\pi/3$, and ε is the dielectric constant, χ is the cell polarization. The value of τ_f can be calculated with the following equation:

$$\tau_f = -\frac{1}{2}\tau_\varepsilon - \alpha_L \quad (4)$$

where τ_ε is the dielectric constant frequency temperature coefficient, α_L is the thermal expansion coefficient. Combining Equation (1) and Equation (2), the following equation can be obtained:

$$\tau_f = -\frac{\varepsilon}{6\alpha}\frac{\partial\chi}{\partial T} + \left(\frac{\varepsilon}{2} - 1\right)\alpha_L \quad (5)$$

The dielectric constant and the thermal expansion coefficient can be approximate as a fixed value, so the value of τ_f is approximate in inverse proportion with the cell polarization. The calculated cell polarization and τ_f of the CTLA ceramics with different amounts of Nd_2O_3 sintered at 1450 °C for 4 h are shown in Fig. 6. Meanwhile, the crystal cell volume has the same tendency with relative densities. Constrained by symmetry operators of $P4_22_12$ (No. 94), the lattice parameter and χ_{cal} of the CTLA ceramics with different amounts of Nd_2O_3 were obtained from the crystal cell refinement as shown in Table 3.

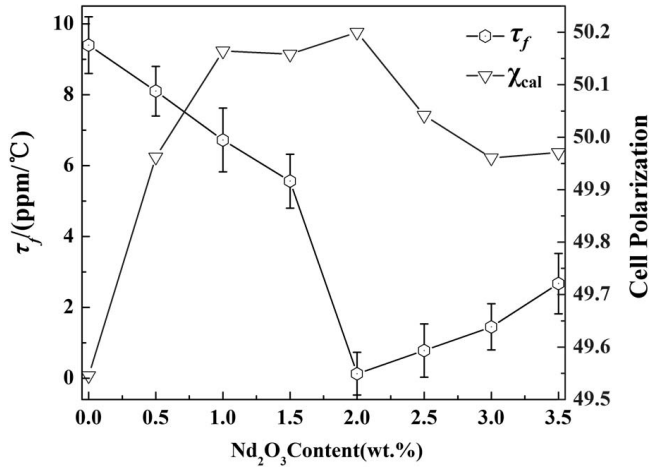

Fig. 6: The calculated cell polarization and τ_f of CTLA ceramics with different amounts of Nd_2O_3sintered at 1450 °C for 4 h.

(4) Microstructure

Fig. 7 shows SEM images of polished and thermally etched surfaces of CTLA samples sintered at 1450 °C for 4 h. Well-densified and homogeneous structures are observed in all samples, which means there has been good grain growth process during sintering. The grain size of undoped the CTLA ceramics is only 5.75 μm. The grain size of the CTLA ceramics is clearly improved with the addition of Nd_2O_3. Moreover, the grain size of the ceramics increases until it reaches a maximum value and then decreases with further increase in the Nd_2O_3 addition. The biggest grain size is 9.25 μm at 2 wt% Nd_2O_3.

Table 3: The lattice parameter and χ_{cal} of the CTLA ceramics with different amounts of Nd_2O_3sintered at 1450 °C for 4 h.

Sample name	Refined (Å)		Vol ($Å^3$)	χ_{cal}
	A	c		
0 wt%	5.3963	7.5945	221.16	49.54
0.5 wt%	5.4043	7.6385	223.10	49.96
1 wt%	5.4125	7.6609	224.11	50.13
1.5 wt%	5.4130	7.6484	224.23	50.16
2 wt%	5.4135	7.6405	224.69	50.20
2.5 wt%	5.4096	7.6380	223.92	50.04
3 wt%	5.4091	7.6454	223.53	49.98
3.5 wt%	5.4076	7.6427	223.49	49.97

(5) Raman spectra analysis

Raman spectra of the CTLA ceramics with different amounts of Nd_2O_3 are shown in Fig. 8. The effect of cation ordering on vibrational spectra of CTLA ceramics was analyzed using Raman spectroscopy [20]. As it can be seen, there are the same peak positions, but different peak area spectral profiles are clearly observed, which indicates that different crystalline structures likely occur in the ceramics [21]. The ideal simple tetragonal (P422) structure exhibits five Raman-active modes ($2A_{1g}+2B_{2g}+E_g$) and six infrared bands ($2A_{2u}+B_{2u}+3E_u$). As shown in Fig. 7, it is worth noting that the CTLA ceramics have a tetragonal $P4_22_12$ structure, which presents three intense Raman active modes with symmetries ($A_{1g}+2B_{2g}$) and three infrared bands ($A_{2u}+B_{2u}+E_u$). Peaks of 278 and 335 cm^{-1} derive from B_{2g} vibrations (*A*-site cations), and the peak of 794 cm^{-1} derives from A_{1g} vibrations (symmetric stretching of the TiO_6 octahedra) [22]. One Raman active mode with symmetry A_{1g} appeared for the ceramics doped with 2.0 wt% Nd_2O_3, which can be attributed to the A_{1g}-like mode (peak of 394 cm^{-1}) that corresponds to symmetric breathing of oxygen octahedra [23]. With increasing Nd_2O_3 concentration, the bands did not present the same behavior for frequencies, widths, and intensities. However, two infrared active modes with dissymmetry ($A_{2u}+E_u$) (peaks of 374 and 413 cm^{-1}) appeared for the ceramics doped with 3.5 wt% Nd_2O_3. This occurred because some bands are more sensitive to the unit cell volume, others to the tolerance factor, and others to *B*-site ordering, which have different effects on the bands. The peak area increased with increasing Nd_2O_3 concentration when the doping amount was less than 2.0 wt%, which indicated an increase in the long range order (LRO), which is also in agreement with XRD analysis.

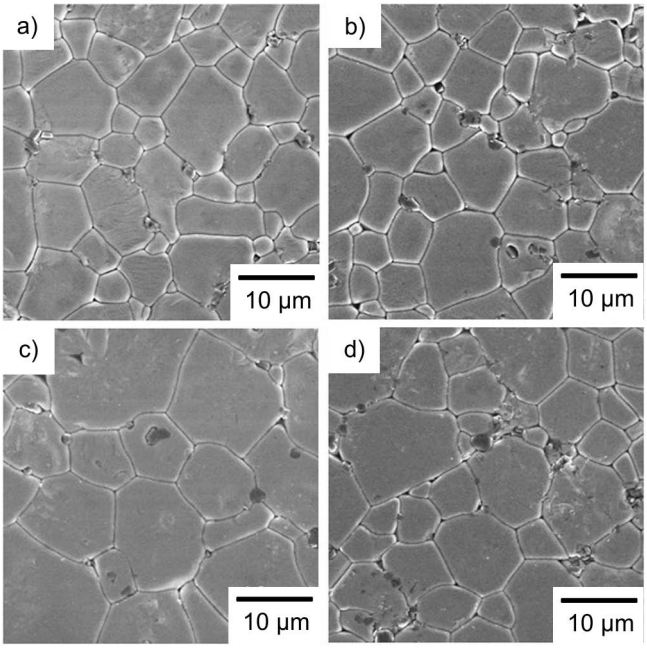

Fig. 7: The SEM images of CTLA ceramics with different amounts of Nd_2O_3sintered at 1450 °C for 4 h: (a) 0 % Nd_2O_3; (b) 0.5 wt% Nd_2O_3; (c) 2.0 wt% Nd_2O_3; (d)3.5 wt% Nd_2O_3.

In addition, the Raman intensity depends on the changes of molecular polarizability in the vibration process. The Raman intensity becomes stronger with the increasing variation of polarization [24], as shown in Fig. 9. Because the peak of 794 cm^{-1} derives from symmetric stretching of the TiO_6 octahedra, as shown in Fig. 8, there are variations in peak intensities (peak of 794 cm^{-1}) with different Nd_2O_3 doping. This indicates that the doping of Nd_2O_3 has an influence on the symmetric stretching of the TiO_6 octahedra in CTLA ceramics, which is also in agreement with the lattice parameter result in Table 3. The Raman intensity (peak of 794 cm^{-1}) of undoped CTLA ceramics is the largest, while the variation of polarization is the largest. The Raman intensities of the CTLA ceramics decrease gradually with Nd_2O_3 addition, the variations of polarization have the same change trend. Moreover, the Raman intensities of the ceramics decrease until they reach the smallest value at 2.0 wt% Nd_2O_3, and at the same time the variation of polarization is at the minimum. Then the Raman intensities of ceramics increase with the increasing Nd_2O_3 addition. The trend of Raman intensity explained that Nd atoms replacing Ca atoms improves the symmetry of the lattice, but Nd atoms replacing La atoms destroys the symmetry of the lattice, these chemical reactions consequently changing the molecular polarizability. The Raman intensity of the ceramic doped with 2.0 wt% Nd_2O_3 was the smallest, which corresponded to the smallest variation of polarization. The minimum variation of polarization demonstrated that the symmetry of the lattice is optimized. In this condition, the dielectric loss of the CTLA ceramics was the lowest and the resonant frequency temperature coefficient is nearly zero. The variations of polarization and peak area at 794 cm^{-1} of CTLA ceramics with different amounts of Nd_2O_3 are shown in Fig. 8. It is demonstrated that the peak area is approximate in direct proportion to the variations of polarization, and the variation of polarization is positively related with cell symmetry. This is also consistent with the results in Table 3.

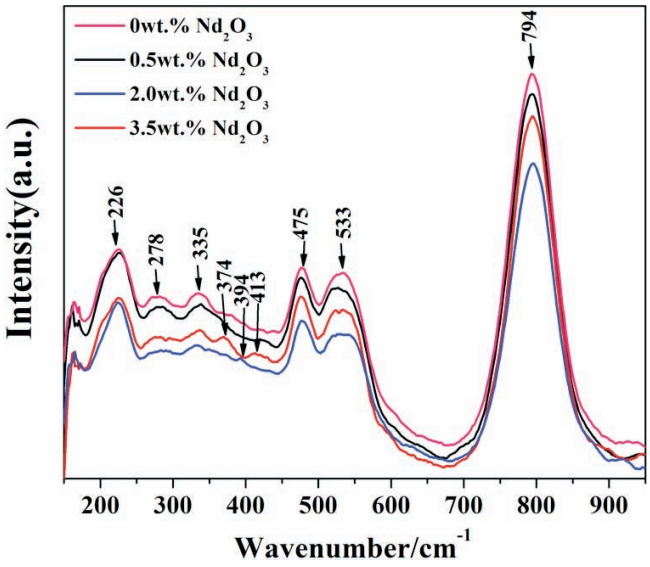

Fig. 8: Room temperature Raman spectra of CTLA ceramics with different amounts of Nd_2O_3 sintered at 1450 °C for 4 h: (a) 0 % Nd_2O_3; (b) 0.5 wt% Nd_2O_3; (c) 2.0 wt% Nd_2O_3; (d) 3.5 wt% Nd_2O_3.

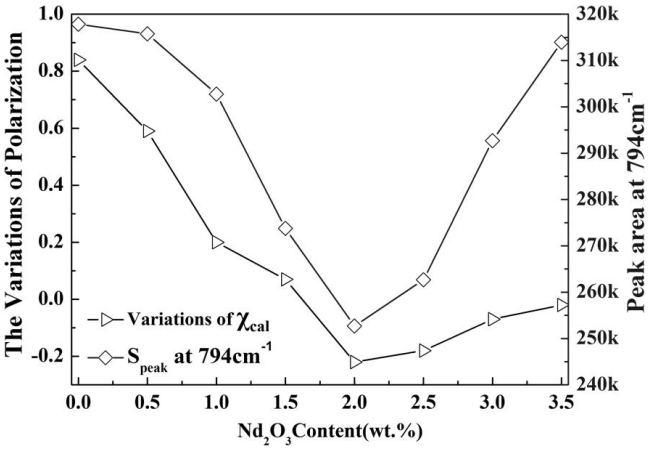

Fig. 9: The variations of polarization and peak area at 794 cm^{-1} of CTLA ceramics with different amounts of Nd_2O_3 sintered at 1450 °C for 4 h.

IV. Conclusions

Well-densified CTLA ceramics were prepared with the addition of Nd_2O_3., the samples sintered at 1450 °C for 4 h with 2.0 wt% Nd_2O_3 addition exhibits $\varepsilon_r = 44.79$, $Q \times f = 37454$ GHz, $\tau_f = 0.13$ ppm/°C at 4.0 GHz whereas the undoped sample exhibits $\varepsilon_r = 46.72$, $Q \times f = 36{,}718$, $\tau_f = 11.49$ ppm/°C. A structural study (XRD) showed that CTLA ceramics have a tetragonal $P4_22_12$ (No. 94) structure at room temperature, the (200) crystal plane is obvious to the small angle deviation trend. The Ca^{2+} in ABO_3 perovskite-type structure at the A sites were substituted by Nd^{3+} when the Nd_2O_3 content was less than 2.0 wt%. However, the La^{3+} at the A sites would also be substituted by Nd^{3+} when the Nd_2O_3 content was more than 2.0 wt%. The Rietveld refinement results also proved this process. The microwave dielectric properties of CTLA ceramics were affected by the presence of Nd_2O_3 additions. The change in the dielectric constant was similar to the

change in the relative density. The value of τ_f can be adjusted by changing the cell polarization for the dielectric constant. The microstructure images show well-densified and homogeneous structures in all samples. In addition, Raman spectroscopy can effectively explain the change in dielectric properties and lattice vibration. A total of three Raman-active bands and three IR phonon modes were observed, in good agreement with group-theoretical calculations for a tetragonal $P4_22_12$ structure. The Raman peak area increases with increasing Nd_2O_3 concentration when the doping amount is less than 2.0 wt%, which indicates a decrease in the long range order, also in agreement with XRD analysis.

Acknowledgements

This work was supported by Priority Academic Program Development of Jiangsu Higher Education Institutions (PAPD) and Science and Technology projects of Guangdong Province (2011A091103002).

References

1 Zhang, X., Zhang, Y., Zhang, J., Peng, B., Xie, Z., Yuan, L., Yue, Z., Li, L.: Microwave dielectric properties and thermally stimulated depolarization currents study of (1-x)$Ba_{0.6}Sr_{0.4}La_4Ti_4O_{15-x}TiO_2$ ceramics, *J. Am. Ceram. Soc.*, **97**, 3170 – 3176, (2014).

2 Ma, P.P., Yi, L., Liu, X.Q., Li, L., Chen, X.M.: Effects of mg substitution on Order/Disorder transition, microstructure, and microwave dielectric characteristics of $Ba((Co_{0.6}Zn_{0.4})_{1/3}Nb_{2/3})O_3$ Complex perovskite ceramics, *J. Am. Ceram. Soc.*, **96**, 1795 – 1800, (2013).

3 Yao, G., Liu, P., Zhang, H.: Low-temperature sintering and microwave dielectric properties of $(Mg_{0.95}Zn_{0.05})_2(Ti_{0.8}Sn_{0.2})O_4$–$(Ca_{0.8}Sr_{0.2})TiO_3$ Composite ceramics, *J. Am. Ceram. Soc.*, **96**, 3114 – 3119, (2013).

4 Ghosh, B., Halder, S., Sinha, T.P.: Dielectric relaxation and collective vibrational modes of double-perovskites A_2SmTaO_6 (A = ba, sr and Ca), *J. Am. Ceram. Soc.*, **97**, 2564 – 2572, (2014).

5 Guo, J., Zhou, D., Zou, S.-L., Wang, H., Pang, L.-X., Yao, X.: Microwave dielectric ceramics Li_2MO_4-TiO_2 (M = Mo, W) with low sintering temperatures, *J. Am. Ceram. Soc.*, **97**, 1819 – 1822, (2014).

6 Su, C., Fang, W., Wei, Z., Tang, Y., Fang, L.: Microwave dielectric properties of $MLi_2Ti_6O_{14}$ [M=Ba and Sr] ceramics and their compatibility with sliver, *J. Am. Ceram. Soc.*, **97**, 3740 – 3743, (2014).

7 Kipkoecha, E.R., Azough, F., Freer, R., Leach, C.,Thompson, S.P., Tang, C.C.: Structural study of $Ca_{0.7}Nd_{0.3}Ti_{0.7}Al_{0.3}O_3$ dielectric ceramics using synchrotron X-ray diffraction, *J. Eur. Ceram. Soc.*, **23**, 2677 – 2682, (2003).

8 Jancar, B., Suvorov, D., Valant, M., Drazic, G.: Characterization of $CaTiO_3$-$NdAlO_3$ dielectric ceramics, *J. Eur. Ceram. Soc.*, **23**, 1391 – 1400, (2003).

9 Pashkin, A., Kamba, S., Berta, M., Petzelt, J., Csete de Gyorgyfalva, G.D.C., Zheng, H., Bagshaw, H., Reaney, I.M.: High frequency dielectric properties of $CaTiO_3$-based microwave ceramics, *J. Phys. D: Appl. Phys.*, **38**, 741 – 748, (2005).

10 Khalyavin, D.D., Salak, A.N., Senos, A.M.R. *et al.*: Structure sequence in the $CaTiO_3$-$LaAlO_3$ microwave ceramics – revised, *J. Am. Ceram. Soc.*, **89**, [5], 1721 – 1723, (2006).

11 Pang, L.-X., Zhou, D., Guo, J., Yue, Z.-X., Yao, X.: Microwave dielectric properties of $(Li_{0.5}Ln_{0.5})MoO_4$ (Ln = Nd, Er, Gd, Y, Yb, Sm, and Ce) ceramics, *J. Am. Ceram. Soc.*, **98**, 130 – 135, (2015).

12 Nenasheva, E.A., Mudroliubova, L.P., Kartenko, N.F.: Microwave dielectric properties of ceramics based on $CaTiO_3$-$LnMO_3$ system (Ln-La, Nd; M-Al, Ga), *J. Eur. Ceram. Soc.*, **23**, 2443 – 2448, (2003).

13 Suvorov, D., Valant, M., Jancar, B. *et al.*: $CaTiO_3$-based ceramics: microstructural development and dielectric properties, *Acta Chim.Slov.*, **48**, [1], 87 – 100. (2001).

14 Zhang, J., Yue, Z., Zhou, Y., Zhang, X., Li, L.: Microwave dielectric properties and thermally stimulated depolarization currents of (1 – x)$MgTiO_3$–$_xCa_{0.8}Sr_{0.2}TiO_3$Ceramics, *J. Am. Ceram. Soc.*, **98**, 1548 – 1554, (2015).

15 Ravi, G.A., Azough, F., Freer, R.: Effect of Al_2O_3 on the structure and microwave dielectric properties of $Ca_{0.7}Ti_{0.7}La_{0.3}Al_{0.3}O_3$, *J. Eur. Ceram. Soc.*, **27**, 2855 – 2859, (2007).

16 Zhou, Y., Meng, S., Wu, H., Yue, Z.: Microwave dielectric properties of $Ba_2Ca_{1-x}Sr_xWO_6$ double perovskites, *J. Am. Ceram. Soc.*, **94**, 2933 – 2938, (2011).

17 Zhang, S.L., Ma, P.P., Liu, X.Q., Chen, X.M.: Structure and microwave dielectric characteristics of $Ca[(Ga_{1/2}Nb_{1/2})_{1-x}Ti_x]O_3$ ceramics, *J. Am. Ceram. Soc.*, **98**, 3185 – 3191, (2015).

18 Shannon, R.D.: Revised effective ionic radii and systematic studies of interatomic distances in halides and chalcogenides, *Acta. Cryst.*, **A32**, 751 – 767, (1976).

19 Huang, J., Zhou, D.X., Hu, M.Z., Wang, H. :The preliminary study of the improvement principle of Ln rare earth element on microwave dielectric ceramics, *J. Huazhong Univ. Sci.*, **33**, [2], 19 – 21.

20 Lowndes, R., Azough, F., Cernik, R., Freer, R.: Structures and microwave dielectric properties of $Ca_{(1-x)}Nd_{2x/3}TiO_3$ ceramics, *J. Eur. Ceram. Soc.*, **32**, 3791 – 3799, (2012).

21 Xi, H.H., Zhou, D., Xie, H.-D., He, B., Wang, Q.-P.: Raman spectra, infrared spectra, and microwave dielectric properties of low-temperature firing $[(Li_{0.5}Ln_{0.5})_{1-x}Ca_x]MoO_4$ (Ln = sm and Nd) solid solution ceramics with scheelite structure, *J. Am. Ceram. Soc.*, **97**, 587 – 593, (2014).

22 Dias, A., Lage, M.M., Khalam, L.A., Sebastian, M.T., Moreira, R.L.: Vibrational spectroscopy of Ca_2LnTaO_6 (Ln = lanthanides, Y, and In) and Ca_2InNbO_6 double perovskites, *Chem. Mater.*, **23**, 14 – 20, (2011).

23 Dias, A., Khalam, L.A., Sebastian, M.T., Lage, M.M., Matinaga, F.M., Moreira, R.L.: Raman scattering and infrared spectroscopy of chemically substituted Sr_2LnTaO_6 (Ln) lanthanides, Y, and In) double perovskites, *Chem. Mater.,* **20**, 5253 – 5259, (2008).

24 Kaminskii A.A.: Achievements in the field of physics and spectroscopy of activated laser crystals, *Phys. Status Solidi A*, **87**, 11 – 57, (1985).